



Eco-physiological evaluation of *Stele Transversal Area 1* for rice root anatomy and shoot growth

Phoura Y, Akihiko Kamoshita, Mariko Norisada & Vivek Deshmukh

To cite this article: Phoura Y, Akihiko Kamoshita, Mariko Norisada & Vivek Deshmukh (2020) Eco-physiological evaluation of *Stele Transversal Area 1* for rice root anatomy and shoot growth, Plant Production Science, 23:2, 202-210, DOI: [10.1080/1343943X.2020.1727754](https://doi.org/10.1080/1343943X.2020.1727754)

To link to this article: <https://doi.org/10.1080/1343943X.2020.1727754>



© 2020 The Author(s). Published by Informa UK Limited, trading as Taylor & Francis Group.



[View supplementary material](#)



Published online: 19 Feb 2020.



[Submit your article to this journal](#)



Article views: 608



[View related articles](#)



Citing articles: 1 [View citing articles](#)

Eco-physiological evaluation of *Stele Transversal Area 1* for rice root anatomy and shoot growth

Phoura Y^{a,b}, Akihiko Kamoshita^b, Mariko Norisada^b and Vivek Deshmukh^b

^aGraduate School of Agricultural and Life Sciences, The University of Tokyo, Tokyo, Japan; ^bAsian Natural Environmental Science Center, The University of Tokyo, Tokyo, Japan

ABSTRACT

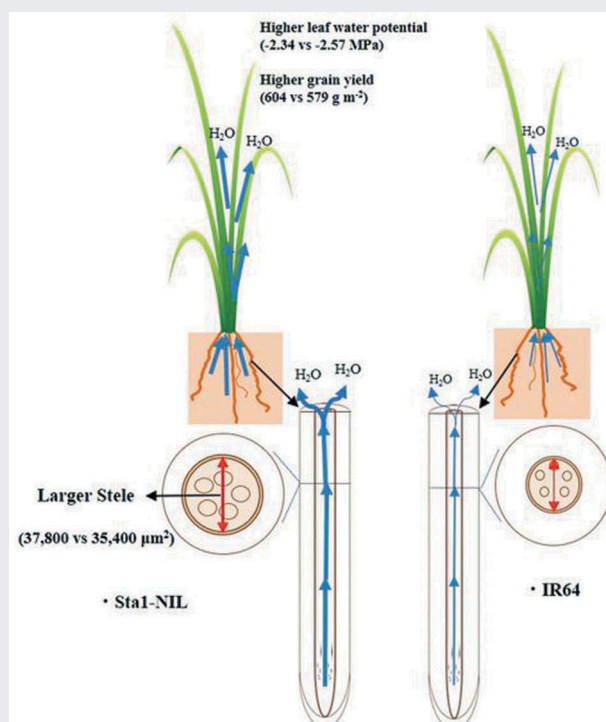
Larger stele size with greater xylem area or endodermis thickness in rice roots may lead to higher plant water status and maintain yield. *Sta1-NIL*, a near-isogenic line of IR64 introgressed with *Stele Transversal Area 1* (*Sta1*), a quantitative trait locus controlling stele transversal area (STA) was investigated together with IR64 for their root anatomy and physiological parameters, at seedling, heading and maturity stages in greenhouse and fields of water deficit and well-watered conditions in 2017 and 2018. Combined analysis of STA from nine observations of overall four experiments showed that STA was increased by 7% (35,400 to 37,800 μm^2) by the introduction of *Sta1* into IR64. Total late metaxylem area also increased by 6% (5,840 to 6,180 μm^2), which came mainly from its single area rather than its number, whereas small increase in endodermis thickness was also noted. Genotype \times observation for STA was marginal, but *Sta1-NIL* had larger STA under water deficit environments. *Sta1-NIL* also maintained higher mid-day leaf water potential (-2.34 ± 0.3 MPa) than IR64 (-2.57 ± 0.3 MPa). Meta-analysis of seven experiments under 14 environments showed tendency of the positive effect of *Sta1* on grain yield increment (579 to 604 g m^{-2}), which came from the increment of harvest index. This study indicated the importance of wider stele size for maintenance of higher plant water status and yield across different water regimes.

ARTICLE HISTORY


Received 25 September 2019
Revised 7 December 2019
Accepted 26 January 2020

KEYWORDS

Stele Transversal Area 1;
ecophysiology; rice; root
anatomy; leaf water
potential



CONTACT Akihiko Kamoshita  akamoshita@anesc.u-tokyo.ac.jp

 The supplemental data for this article can be accessed [here](#).

© 2020 The Author(s). Published by Informa UK Limited, trading as Taylor & Francis Group.

This is an Open Access article distributed under the terms of the Creative Commons Attribution License (<http://creativecommons.org/licenses/by/4.0/>), which permits unrestricted use, distribution, and reproduction in any medium, provided the original work is properly cited.

1. Introduction

Rice is a semi-aquatic plant with a shallow and thin root system compared with dryland crops such as wheat and corn. Investigation of rice root traits and their improvement have been less studied compared to aboveground traits because of difficulty in phenotyping (Voss-Fels, Snowdon & Hickey, 2018). Genetic variation in rice root traits has been reported such as root thickness (Babu et al., 2001) and deep rooting (Nemoto, Suga, Ishihara & Okutsu, 1998), and the latter has been shown to be useful for drought avoidance (Kato et al., 2007; Yoshida & Hasegawa, 1982) and for water-saving (Deshmukh, Kamoshita, Norisada & Uga, 2017) to lead to higher yield (Uga et al., 2013). However, studies of root anatomical traits are less reported probably due to its tedious and time-consuming phenotyping (Atkinson & Wells, 2017; Burton, Williams, Lynch & Brown, 2012; Chopin, Laga, Huang, Heuer & Miklavcic, 2015; Uga, Okuno & Yano, 2008).

Radial anatomy of individual roots is composed of three layers, epidermis, cortex, and stele (Morita & Nemoto, 1995; Rebouillat et al., 2009). Stele is a vascular cylinder that contains xylem, which transports water from root to shoot. Genotypic variation in stele size has been reported in rice (Kondo, Aguilar, Abe & Morita, 2000; Terashima, Hiraoka & Nishiyama, 1987; Uga et al., 2008). Traditional upland *japonica* cultivars showed the largest stele, stele ratio, and late metaxylem vessel diameters, followed by modern upland *japonica*, *aus* and *indica* cultivars (Kondo et al., 2000). Uga et al. (2009) found larger transversal areas of the stele and late metaxylem in upland *japonica* than *indica* and lowland *japonica* rice among Asian rice accessions.

Wider stele with greater xylem area may lead to higher plant water status under water deficit due to higher hydraulic conductivity. Richards and Passioura (1989) reported smaller xylem vessels (indicating smaller stele size) reduced water use of wheat under drought, saved more water during grain filling to attain higher grain yield. Yambao, Ingram and Real (1992) described larger xylem diameters were associated with higher axial conductance, thereby enhancing water uptake capacity in rice. Rieger and Litvin (1999) reported contrasting root anatomy (smaller cortex and bigger stele size) contributed to root hydraulic conductivity among five woody and herbaceous species. Sibounheuang, Basnayake and Fukai (2006) highlighted higher leaf water potential in rice lines with bigger xylem diameters and stem areas. Henry, Cal, Batoto, Torres and Serraj (2012) discussed the possibility of the wider stele was associated with thicker suberized endodermis, which could retain more water under water-limiting conditions. Jeong et al. (2013) reported two rice mutants with larger root diameters

had larger stele size with more stele cell number and higher grain yield under drought, but without quantifying plant physiological responses. Moreover, Kadam, Yin, Bindraban, Struik and Jagadish (2015) found the larger stele ratio to root diameter in drought-resistant cultivars in both rice and wheat. Hazman and Brown (2018) found conserved stele area and heavy lignified stele under drought in rice. However, no studies have ever shown a clear relationship between wider stele size and improved plant physiological functions (e.g., indicated by higher leaf water potential, stomatal conductance, and photosynthetic rate, and/or lower carbon isotope composition ($\delta^{13}\text{C}$)) and improved growth and production under water deficit.

Quantitative trait locus (QTL) underlying natural variation in stele and xylem transversal area of rice roots was found from a cross between the lowland *indica* variety 'IR64' with thinner root stele transversal area (STA) and the traditional tropical upland *japonica* variety 'Kinandang Patong' with thicker STA (Uga et al., 2008). Two QTLs for STA were detected on chromosome 2 and 9 with the nearest markers RM262 and ID07_14, respectively. Uga, Okuno and Yano (2010) conducted fine mapping of *Stele Transversal Area 1* (*Sta1*), a QTL of STA on the chromosome 9 between markers RM566 and RM24334, and developed a near-isogenic line called *Sta1-NIL* that has the *Sta1* region homozygous for the 'Kinandang Patong' allele, which brought about 25% increase in STA and 15% increase in total late metaxylem area when compared with the line homozygous for 'IR64' allele under upland condition. Deshmukh et al. (2017) evaluated *Sta1* for grain yield under flooded lowland, alternative-wetting-and-drying lowland, and rainfed upland conditions with higher harvest index but did not quantify any root anatomical traits such as stele transversal area (STA) and other anatomical traits. The originality of this study was to quantify the effects of *Sta1* on the phenotype of root anatomical traits under different environments including greenhouse and fields. This study also aimed to quantify the effects of *Sta1* on shoot growth including plant water status, and meta-analysed yield from different experiments.

2. Materials and methods

2.1. Plant materials

IR64 and *Sta1-NIL* were grown to compare its root anatomy and shoot growth. IR64 is a modern lowland cultivar (subsp. *indica*) developed by International Rice Research Institute (IRRI) in the Philippines and widely grown in South and Southeast Asia (Mackill & Khush, 2018). *Sta1-NIL* (BC₅F₄) used in this study was a cross

between IR64 and Kinandang Patong by five repeated marker-assisted backcrosses to eliminate non-target regions (Uga et al., 2008, 2010).

2.2. Experimental design

Experiments were conducted at the Institute for Sustainable Agro-ecosystem Services, The University of Tokyo, Nishitokyo, Japan (35°43'N, 139°32'E) from April to October 2017 and from April to July 2018. The site has volcanic ash soil of silty Kanto loam type (Humic Andosol) with dark humic silty topsoil (0–35 cm) and red-brown silty clay subsoil (below 35 cm) (Yamagishi, Nakamoto & Richner, 2003). Average values of soil chemical properties from the fields (N = 9) were pH 6.6 ± 0.1 , electrical conductivity $0.098 \pm 0.026 \text{ mS cm}^{-1}$, cation exchange capacity $37.6 \pm 1.6 \text{ meq } 100 \text{ g m}^{-1}$, and bulk density $0.90 \pm 0.05 \text{ g cm}^{-3}$ (Deshmukh et al., 2017).

In 2017, plants were grown into flooded lowland (i.e., well-watered (WW)) and rainfed upland (i.e., water deficit (WD)) fields (12 m × 16 m per treatment) separated by a mounted levee in a randomized complete block design with four replications per field. Seeds were sown into cell trays on 28 April and seedlings were transplanted with one plant per hill at 15 cm × 30 cm spacing on 19–21 May. P₂O₅ and K₂O were applied each at 10 g m⁻² as a basal fertilizer on 8 May with five subsequent N fertilization rates; 6 g m⁻² after transplanting (26 May) and 3 g m⁻² on early tillering (20 June), mid-tillering (3 July), panicle

initiation (24 July) and before heading (14 August), respectively. Pre-emergence herbicides were applied to control weeds in the early growth stages, and plots were regularly manually weeded until the grain-filling stage. After transplanting, there was no irrigated water but rainfall to the WD condition until harvesting on 3 October (Exp. S2; Table 1; Exp. Y7; Table 2). A preliminary greenhouse experiment was also conducted; seeds of the two genotypes were sown into cell trays with one seed per cell on 21 June and sampled on 14 July or 23 days after sowing (DAS) (Exp. S1; Table 1).

In 2018, greenhouse experiments using polyvinyl pipes (PVCs) and field experiments using a modified basket method (Oyanagi, Nakamoto & Wada, 1993; Ramalingam, Kamoshita, Deshmukh & Uga, 2017) were conducted. In greenhouse, nine PVCs (10.9 cm internal diameter, 50 cm depth, with a small hole at the bottom for water inlet from the pool mentioned below) per genotype were filled with nursery soil (N-P-K 6.4-8.9-6.4 g m⁻² respectively) up to 45 cm height and placed into a pool (1.5 m × 4.5 m, 0.10 m depth) in a randomized block design with three replications. Water was irrigated from both the top and the bottom of the pot; 0.3 L of water from the top was daily given until the first sampling on 22 June (36 days after transplanting (DAT)), thereafter every 2 days until 19 July (63 DAT) (Exp. S3; Table 1), while sufficient amount of water was daily given to the pool of 0.1 m depth, which accommodated eight pots/pool. Seeds were sown into cell trays on 23 April and transplanted one plant per PVC on 17 May.

Table 1. Experimental environments for stele observation and physiological measurements. There were four experiments conducted in 2017 and 2018 under both greenhouse and WD and WW field conditions (S1–S4). The stele was observed in nine combinations of environments and timings at the seedling stage (23 DAS), heading stage (102 DAT), and maturity stage in 2017, and at 36 and 63 DAT in 2018 as well. For physiological measurements, LWP, $\delta^{13}\text{C}$ and photosynthetic parameters were measured 5 times at the heading stage (except $\delta^{13}\text{C}$ at maturity) in 2017 and 63 DAT in 2018.

Exp.	Year	Environments	Stele observation (9 observations in total)	Physiological measurements (5 measurements in total)
S1	2017	Greenhouse	Seedling (23 DAS)	–
S2	2017	Fields (WW, WD)	Heading (102 DAT), Maturity	LWP (107 DAT), $\delta^{13}\text{C}$, P _n , T _r , TE, g _s (95–96 DAT)
S3	2018	Greenhouse	36 & 63 DAT	LWP, $\delta^{13}\text{C}$, P _n , T _r , TE, g _s (63 DAT)
S4	2018	Fields (WW, WD)	63 DAT	LWP, $\delta^{13}\text{C}$, P _n , T _r , TE, g _s (61 DAT)

WD: water deficit; WW: well watered; DAS: days after sowing; DAT: days after transplanting; LWP: leaf water potential (by pressure chamber); $\delta^{13}\text{C}$: carbon isotope composition (by EA/IRMS); P_n: photosynthetic rate; T_r: transpiration rate; TE: transpiration efficiency (P_n/T_r); g_s: stomatal conductance (by LI-6400).

Table 2. Experimental environments, N fertilization rates and dates of sowing, transplanting and harvest for meta-analysis of grain yield, aboveground biomass and harvest index of IR64 and Sta1-NIL under 14 environments from 7Y experiments (Y1–Y7).

Exp.	Years	Environments (14 in total)	N fertilization rates (kg N/ha)	Sowing-transplanting-harvesting dates	References
Y1	2013	AWD, FL, RU	60	4/22 – 6/5, 5, 5/29 – 10/7, 9/30, 10/14	Deshmukh et al. (2017)
Y2	2014	AWD, FL, RU	60	4/28 – 5/23, 26, 28 – 10/10, 11	Yaginuma (2017)
Y3	2014	FL	80	4/28 – 5/19 – 9/17	
Y4	2015	FL*	69*	4/12 – 5/3 – 9/17	
Y5	2016	FL*	61*	4/27 – 5/18 – 9/28	
Y6	2016	AWD*, FL*, RU*	60*	4/14 – 5/29 – 10/10, 11/3	Y et al. (unpublished data)
Y7	2017	FL, RU	180	4/28 – 5/19, 21 – 10/3, 27	

AWD: alternative wetting and drying; FL: flooded lowland; RU: rainfed upland. *: N fertilization was applied by deep placement as well as conventional surface placement (total two treatments), to be counted as two environments.

The PVCs were rotated every 2 weeks to get uniform sunlight.

In field (Exp. S4; Table 1), three of 15 plants per plot (90 cm × 150 cm) were embedded with plastic baskets (9.5 cm height, 7.5 cm and 4.8 cm top and bottom radii) in WD and WW fields (6 m × 10.5 m) in a randomized complete block design with four replications per field with basal fertilization (N-P₂O₅-K₂O 6-9-8 g m⁻²). Seeds were sown into cell trays on 23 April and the seedlings were transplanted with one plant per hill (30 × 30 cm) into WW on 14 May and WD on 22 May. In order to avoid possible exposure to heavy rainfall during rainy season, WD field in 2018 was covered with vinyl shelter without providing no water for 4 weeks from 22 June (31 DAT). The plants were harvested on 24 July (63 DAT).

In the field experiments of 2017 and 2018 (Exp. S2 and S4), daily minimum and maximum temperatures, daily cumulative solar radiation, and daily rainfall were measured from April to October in 2017 and May to August in 2018 by a weather station installed 100 m away from fields. Rainfall data were not collected properly due to the instrument disorder and it was replaced from Fuchu weather station situated 7.85 km away from the field (www.data.jma.go.jp). The daily air temperature was 22.15 ± 3.4°C (mean ± SD) in 2017 and 25.4 ± 4.68°C in 2018. The daily minimum and maximum air temperatures were 17.9 ± 5.6 and 27.2 ± 5.8°C in 2017 and 20.1 ± 4.9 and 30.7 ± 5.4°C in 2018. Daily solar radiation was 15.2 ± 7.9 MJ m⁻² in 2017 and 18.2 ± 7.5 MJ m⁻² in 2018. Total seasonal rainfall was 578 mm from 26 April to 3 October in 2017 and 222 mm from 14 May to 24 July in 2018 (Figure S1). Soil water potential was missed in 2017 but

the level of water deficit was considered to be severe from the level of yield reduction. In 2018 soil water potential at 10-cm soil depth was -23 kPa after 4 weeks of excluding rainfall in the WD field using a tensiometer (Water Mark WM-100, Spectrum Technologies Inc.).

2.3. Measurements

2.3.1. Root stele transversal area

Nodal roots from field experiments were randomly selected based on their growth angle from the basket (Exp. S2 & S4; Table 1). The sides of the baskets were divided into two groups of angles from the horizontal, measured from the centre of the basket's top surface: 0–45°, shallow angle roots, and 45–90°, deep angle roots (Figure 1(a)). After removing from the basket, 3 to 5 similar roots from each angle were opted for root anatomical analysis. Nodal roots for greenhouse experiments were sampled from the 3rd highest rooting node from the top of the main stem (Exp. S1 & S3; Table 1), according to previous studies (Terashima et al., 1987; Uga et al., 2008).

The root samples were then immersed in FAA solution (5% formalin, 5% acetic acid, 45% ethanol and 45% H₂O) until sectioning. The roots were dissected with a plant microtome (MTH-1; Nippon Medical & Chemical Instruments Co., Ltd., Osaka, Japan) at 2–3 cm from base (Figure 1(a,b)), stained with Coomassie brilliant blue/Toluidine blue and examined under a fluorescence and phase contrast microscope (BX53, Olympus, Hicksville, NY, USA). The cellSens standard software (Olympus) was used to capture the microscopic images. Root transversal area

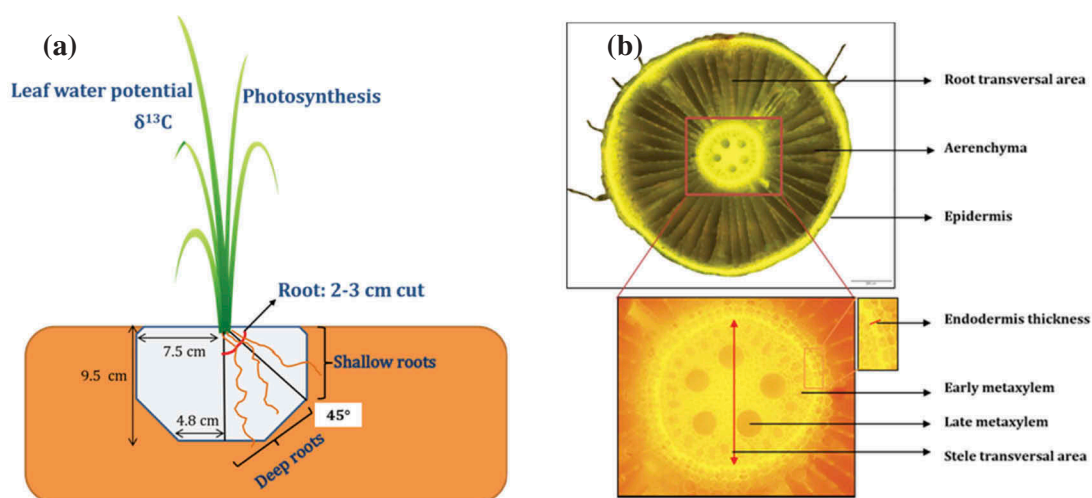


Figure 1. Sampling methods in the fields for stele observation and physiological measurements. (a) Shallow and deep roots were sampled from the basket based on angle and cut at 2–3 cm from base for stele size observation, as well as photosynthesis parameters, leaf water potential (LWP), and $\delta^{13}\text{C}$. (b) Root and stele dissection at 4X and 10X magnifications of a phase-contrast microscope.

(RTA), stele transversal area (STA), total late metaxylem number (LMXN) and area (LMXA), and endodermis thickness (ETH) were recorded using *ImageJ 1.51t* (NIH, Bethesda, MD, USA) (Abramoff, Magalhães & Ram, 2005; Schneider, Rasband & Eliceiri, 2012). The %STA or STA ratio was calculated as $STA/RTA \times 100$ and single late metaxylem area (sLMXA) as $LMXA/LMXN$.

Root anatomical traits were observed on nine occasions; five in 2017 (Exp. S1 and S2) and the rest in 2018 (Exp. 3 and S4) (Table 1).

2.3.2. Leaf water potential

Leaf water potential (LWP) was measured (Figure 1(a)) using a pressure chamber (Daiki Rika Kogyo Co., Ltd., Tokyo, Japan) in 2017 and a Model 600-EXP pressure chamber (PMS Instrument Company, Albany, OR, USA) in 2018, respectively. Fully expanded leaves were sampled in total of five different environments and timings; two environments on 107 DAT in 2017, one greenhouse environment on 63 DAT and two environments on 61 DAT in 2018 (Table 1). Each leaf was cut about 2–3 cm below the junction between the leaf sheath and leaf blade and covered in a wet towel until measurement. Around 3–4 leaves were placed together into the pressure chamber for the measurement. In 2017, LWP of each genotype and environment was measured 3 times from 9:30 to 12:30 to 15:30 and averaged into one mid-day measurement. In 2018, LWP measurements were conducted at 9:00–11:00 in the greenhouse and at 9:00–13:00 in WW and WD fields. Pressure was applied to the leaves until water bubbles appeared at the cut surface.

2.3.3. Photosynthetic parameters

Photosynthetic parameters such as photosynthetic rate (P_n), transpiration rate (T_n), transpiration efficiency (TE), and stomatal conductance (g_s) were measured using portable photosynthetic system LI6400 (LICOR, Lincoln, USA) (Figure 1(a)). The measurements were taken on the flag leaf in two environments at 95–96 DAT in 2017 and in one greenhouse environment at 63 DAT and in two environments at 61 DAT in 2018 (in total five combinations of environments and timing) (Table 1). Measurements were taken on clear sunny days from 10:00 to 12:00 in 2017 and from 8:00 to 11:00 in the greenhouse experiment and from 8:00 to 14:00 at WW and WD in the field experiment in 2018. Relative humidity was adjusted to 60–80%, CO_2 of the inlet air was $400 \mu\text{mol mol}^{-1}$ and the block temperature was set to 28°C to 31°C with light source at $1500 \mu\text{mol m}^{-2} \text{s}^{-1}$. The values of reference and sample CO_2 concentration were matched at $400 \mu\text{mol CO}_2 \text{ mol}^{-1}$ every 30 min.

2.3.4. Carbon isotope composition

Carbon isotope composition ($\delta^{13}\text{C}$) was analyzed on shoot straw of three to four plants per treatment at both greenhouse and field experiments (Figure 1(a)). The plant samples were oven dried at 80°C for 3 days and stored under room temperature until grinding into a very fine powder using a fine mill (Heiko sample mill, TI 300, Fujiwara Seisakusho, Ltd. Tokyo, Japan). The $\delta^{13}\text{C}$ values of powdered samples (0.2 mg) were analyzed with an elemental analyzer/isotope ratio mass spectrometer (EA/IRMS, Flash 2000/Delta V Advantage, Thermo Fisher Scientific, Waltham, MA, USA). $\delta^{13}\text{C}$ was determined in five measurements; two at the maturity stage in 2017 and the others at 63 DAT in 2018 (Table 1).

2.3.5. Grain yield

Meta-analysis of the effect of *Sta1* on grain yield (GY), aboveground biomass (AGB), and harvest index (HI) under 14 environments (i.e., three in alternative wetting and drying (AWD), seven in flooded lowland (FL), and four in rainfed upland (RU) conditions) from seven experiments including two previous reports (Deshmukh et al., 2017; Yaginuma, 2017) and unpublished data in 2016 and 2017 with different N fertilization application rates and sowing dates were also conducted comparing IR64 and *Sta1*-NIL (Table 2). In 2016, plants with 30 cm × 15 cm spacing per hill (40 hills in total) were grown into FL, AWD, and RU fields (12 m × 16 m each) separated by a mounted levee in a randomized complete block design with three replications in each water treatments. In 2017, plants with 30 × 15 cm spacing per hill (162 hills in total) were grown into FL and RU fields (12 m × 16 m each) separated by a mounted levee in a randomized block design with four replications per treatment. Surface N fertilizer in Exp. Y1–Y3 and Y7 were applied as normal top-dressing, and surface and deep N fertilizations in Exp. Y4–Y6 were applied as liquid fertilizer at 5 cm and 12 cm belowground, respectively, during the tillering stage.

2.4. Statistical analysis

All data were analyzed in Genstat 18th edition software (VSNi, Hemel Hempstead, UK). General Analysis of Variance (ANOVA) was performed for each root anatomical traits to compare the performances of IR64 and *Sta1*-NIL for combined and meta-analysis. Multiple comparison analysis of the main effects (genotypes and observations/measurement/environments) was conducted using Tukey's test (significance set at $P < 0.05$). The ANOVA and multiple comparison analyses were also used for LWP, photosynthetic parameters, $\delta^{13}\text{C}$, GY, AGB, and HI. Finlay–Wilkinson regression analysis for STA was

also performed across the nine observation environments for the two genotypes.

3. Results

3.1. Root anatomical traits

Based on the combined analysis of root anatomical traits of IR64 and Sta1-NIL under nine observations in Exp. S1–S4 (Table 3), Sta1-NIL had larger STA by 7% (35,400 to 37,800 μm^2), LMXA by 6% (5,840 to 6,180 μm^2) and ETH by 3% (10.9 to 11.2 μm) than IR64. Sta1-NIL also increased %STA by 5% (4.11% to 4.32%) together with the tendency of larger single late metaxylem area by 4% (1,200 to 1,260 μm^2). Table 3 shows significant differences in the nine observations (O) for STA and other root anatomical traits ($P \leq 0.001$), but large difference in STA was observed under WD conditions (Table S1). STA did

not have significant interactive effects of G x O, but Finlay–Wilkinson regression lines indicated the tendency of greater STA in Sta1-NIL than IR64, particularly where the size of STA was larger (e.g., WD environments) (Figure 2).

3.2. Physiological traits

Sta1-NIL had higher midday LWP (-2.34 ± 0.3 MPa) than IR64 (-2.57 ± 0.3 MPa) in combined analysis under five measurements in Exp. S2–S4 (Table 4). Sta1-NIL tended to have lower leaf temperature (Tleaf) (32.6 vs 33.0°C) than IR64. Genotype by measurement interaction for P_n ($P \leq 0.05$) and for $\delta^{13}\text{C}$ ($P \leq 0.10$) was identified, where Sta1-NIL had higher P_n and tendency of lower $\delta^{13}\text{C}$ under two measurement occasions in the 2018 greenhouse experiment and the WD treatment in 2017 experiment (Table 5).

Table 3. Root anatomy of IR64 and Sta1-NIL under nine observations in Exp. S1–S4 in the combined analysis.

Genotype	RTA ($\times 10^3 \mu\text{m}^2$)	STA ($\times 10^3 \mu\text{m}^2$)	%STA (%)	LMXN	LMXA ($\times 10^3 \mu\text{m}^2$)	ETH (μm)	sLMXA ($\times 10^3 \mu\text{m}^2$)
IR64	903	35.4	4.11	4.85	5.84	10.9	1.20
Sta1-NIL	935	37.8	4.32	4.92	6.18	11.2	1.26
LSD (5%)	48	1.8	0.2	0.2	0.3	0.3	0.1
Genotype (G)	ns	**	*	ns	*	**	ns
Observation (O)	***	***	***	***	***	***	***
G x O	ns	ns	ns	ns	ns	ns	ns

RTA: root transversal area; STA: stele transversal area; %STA: (STA*100)/RTA; LMXN: late metaxylem number; LMXA: total late metaxylem area; ETH: endodermis thickness; sLMXA: single late metaxylem area (LMXA/LMXN). LSD: least significant difference. ANOVA shows significant differences at 5% level (Tukey's test). ***, **, *, +, ns show $P \leq .001, .01, .05, .10$, and no significance, respectively.

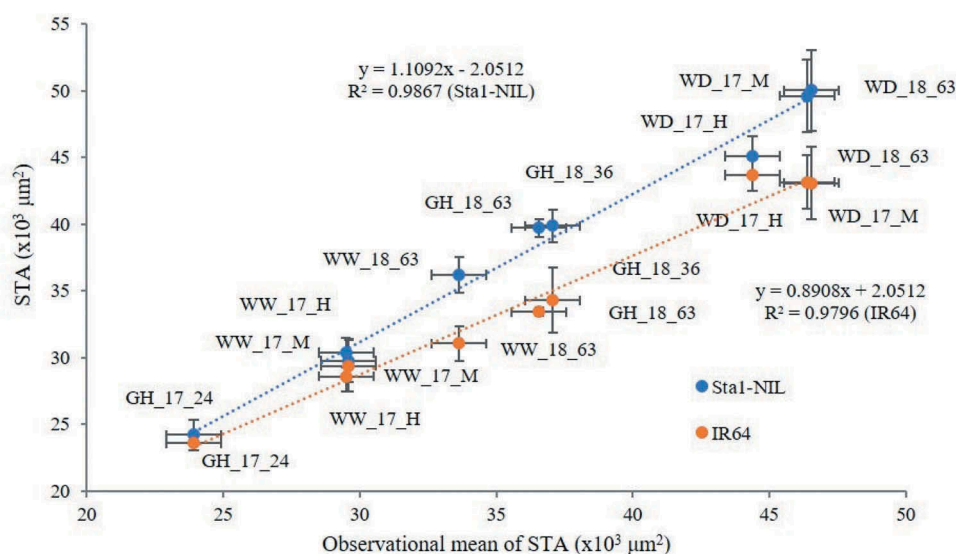


Figure 2. Finlay–Wilkinson regression curves for analysis of genotype by observational interaction for STA across nine observations between the average of two genotypes and IR64 and Sta1-NIL. GH_17_24: greenhouse in 2017 at 24 days after sowing; WD_17_H: water deficit in 2017 at heading stage; WD_17_M: water deficit in 2017 at maturity stage; WW_17_H: well watered in 2017 at heading stage; WW_17_M: well watered in 2017 at maturity stage; GH_18_36: greenhouse in 2018 at 36 days after transplanting; GH_18_63: greenhouse in 2018 at 63 days after transplanting; WD_18_63: water deficit in 2018 at 63 days after transplanting; WW_18_63: well watered in 2018 at 63 days after transplanting. Error bars are standard error values.

Table 4. Leaf water potential (LWP), photosynthetic rate (P_n), transpiration rate (T_r), transpiration efficiency (TE), stomatal conductance (g_s) and carbon isotope composition ($\delta^{13}C$) of IR64 and Sta1-NIL under five measurements in greenhouse in 2018 at 63 days after transplanting and water deficit (WD) and well-watered (WW) in 2017 at heading/maturity and 2018 at 63 days after transplanting in Exp. S2–S4 in the combined analysis.

Genotype	LWP (MPa)	P_n ($\mu\text{mol m}^{-2}\text{s}^{-1}$)	T_r ($\text{mol m}^{-2}\text{s}^{-1}$)	TE ($\mu\text{mol CO}_2/\text{mol H}_2\text{O}$)	g_s ($\text{mol m}^{-2}\text{s}^{-1}$)	Tleaf ($^{\circ}\text{C}$)	Tair-Tleaf ($^{\circ}\text{C}$)	$\delta^{13}C$ (‰)
IR64	-2.57 ± 0.3	18.2 ± 1.5	8.42 ± 0.5	2.25 ± 0.2	0.52 ± 0.1	33.0 ± 0.4	1.33 ± 0.1	-29.7 ± 0.1
Sta1-NIL	-2.34 ± 0.3	18.9 ± 1.4	8.08 ± 0.4	2.48 ± 0.3	0.65 ± 0.3	32.6 ± 0.4	1.44 ± 0.1	-29.7 ± 0.1
LSD (5%)	0.2	1.2	0.8	0.4	0.4	0.4	0.2	0.2
Genotype (G)	**	ns	ns	ns	ns	+	ns	ns
Measurement (M)	***	***	***	***	***	***	*	***
G x M	ns	*	ns	ns	ns	ns	ns	+

LWP: leaf water potential; P_n : photosynthetic rate; T_r : transpiration rate; TE: transpiration efficiency (T_r/P_n); g_s : stomatal conductance; Tair: measured leaf temperature, Tleaf: measured leaf temperature; $\delta^{13}C$: carbon isotope composition; LSD: least significant difference. Numbers after means show standard error values. ANOVA shows significant differences at 5% level (Tukey's test). ***, **, *, +, ns show $P \leq .001, .01, .05, .10$, and no significance, respectively.

Table 5. Photosynthetic rate (P_n) and carbon isotope composition ($\delta^{13}C$) of IR64 and Sta1-NIL under two measurements in water deficit in 2017 at the heading/maturity stage (Exp. S2) and greenhouse in 2018 at 63 days after transplanting (Exp. S3) in the combined analysis.

Genotype	P_n ($\mu\text{mol m}^{-2}\text{s}^{-1}$)	$\delta^{13}C$ (‰)
IR64	21.3 ± 0.6	-29.7 ± 0.2
Sta1-NIL	23.7 ± 0.7	-30.0 ± 0.1
LSD (5%)	2.2	0.3
ANOVA	*	+

P_n : photosynthetic rate; $\delta^{13}C$: carbon isotope composition; LSD: least significant difference. Numbers after means show standard error values. ANOVA shows significant differences at 5% level (Tukey's test). ***, **, *, +, ns show $P \leq .001, .01, .05, .10$, and no significance, respectively. (1Y-7Y). ***, **, *, +, ns show $P \leq .001, .01, .05, .10$, and no significance, respectively (Tukey's test). Error bars show standard error values.

3.3. Grain yield

Meta-analysis of the effect of *Sta1* on yield under the 14 environments from seven experiments showed that HI, together with the tendency of GY, was higher in Sta1-NIL than IR64 (Figure 3). Sta1-NIL increased HI from 0.453 to 0.463 and GY from 579 to 604 g m^{-2} (or 25 g m^{-2} or 250 kg ha^{-1}) compared to IR64, while there was no significant increase in AGB. In an individual environment, Sta1-NIL showed higher HI in AWD in 2014 ($P < 0.026$) and 2016 ($P < 0.034$) (Deshmukh et al., 2017; Y, 2019) (Table S2).

4. Discussion

This study quantified the magnitude of the effects of *Sta1* to increase stele size and maintain higher plant water status and yield of IR64. By the introduction of *Sta1* into IR64, STA increased by 7%, accompanied by increase in LMXA by 6% and ETH by 3% based on the combined analysis in all the data in 2 years of the overall four experiments that included both well-watered and water-deficit environments (Table 3; Table S1). The

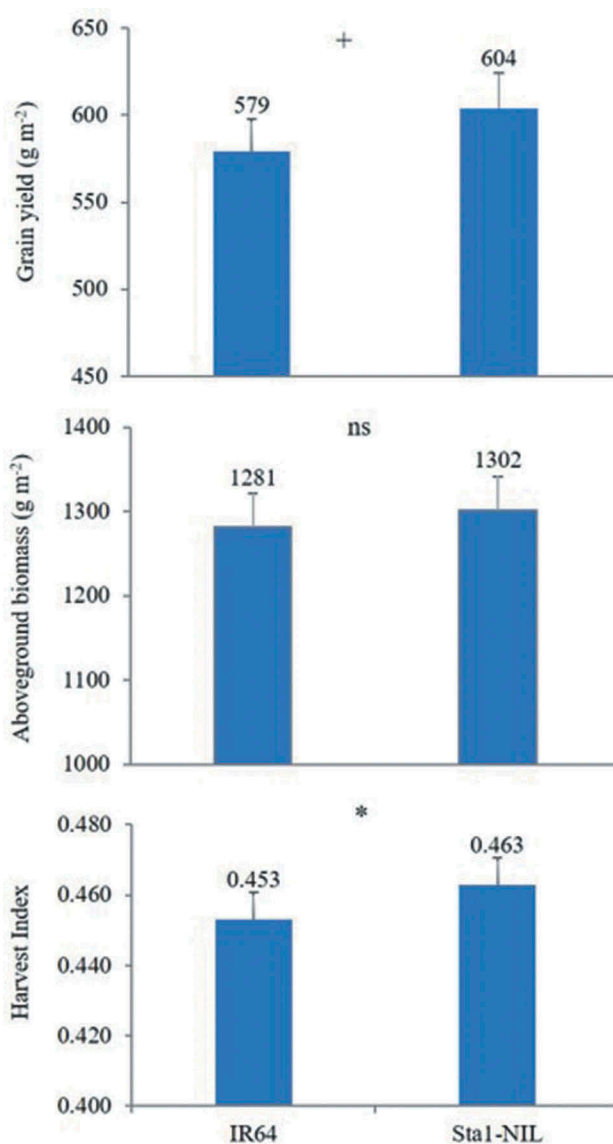


Figure 3. Meta-analysis of the effect of *Sta1* on grain yield, aboveground biomass, and harvest index under 14 environments from seven experiments (Y1–Y7). ***, **, *, +, ns show $P \leq .001, .01, .05, .10$, and no significance, respectively (Tukey's test). Error bars show standard error values.

increased STA was driven by increase in LMXA, consistent with the previous report (Uga et al., 2008). Increased LMXA could be mainly contributed from its single area rather than its number as its single area (sLMXA) was marginally increased by 4%, but not the LMXN (Table 3). Increase in STA could also lead to an increase in ETH since the single endodermis layer circles the stele to protect the stele components such as xylem vessels and prevent water flow backward (Miyamoto, Steudle, Hirasawa & Lafitte, 2001).

The increased stele size for Sta1-NIL contributed to higher LWP (-2.57 ± 0.29 vs -2.34 ± 0.27 MP) as compared with IR64 in overall three experiments (Table 4), the effects of which tended to be larger under water deficit environments (Figure 2). Interestingly, higher P_n and lower $\delta^{13}C$ (more stomatal openness and higher water conductance) for Sta1-NIL than IR64 were also demonstrated under the two environments implied with WD conditions (Table 5); WD of Exp. S2 in 2017 suffered nearly 50% yield reduction compared with WW, and Exp. S3 in 2018 recorded low LWP (-3.83 MPa, data not shown) probably due to the heat in the greenhouse. Sibounheuang et al. (2006) reported rice lines with larger xylem diameter and stem area maintained higher LWP in midday measurements under both glasshouse and field conditions. Thicker ETH affects plant water status (Miyamoto et al., 2001) and may help rice plants to retain more water inside the stele under water deficits (Henry et al., 2012), thereby increasing plant water status. Thus, the significant difference in LWP in our study could be contributed from larger stele size and/or suberized endodermis, but further studies are required in order to confirm this speculation.

Improved plant water status and physiological activity (e.g., LWP, P_n) could lead to higher HI and GY. GY increased by 25 g m^{-2} higher in Sta1-NIL than IR64 in overall seven experiments (Figure 3) with less reduction in HI under some of marginal environments such as AWD in 2014 and 2016 (Table S2). Higher LWP under drought was suggested to reduce spikelet sterility, thereby increasing yield (Jongdee, Fukai & Cooper, 2002). Deshmukh et al. (2017) also showed higher HI of Sta1-NIL than IR64 across different water environments but did not verify the relationship between larger stele size and physiological functions. This study clarified the importance of wider stele size using Sta1-NIL for maintenance of higher plant water status and yield under different water regimes.

Acknowledgments

We thank Dr. Yusaku Uga, Agro-genomics Research Center, National Agriculture, and Food Research Organization,

Tsukuba, Japan, for providing seeds of the Sta1-NIL. We also thank the technical staffs of Institute for Sustainable Agro-ecosystem Services, The University of Tokyo, for their field preparation and Laboratory of Environmental Stress Tolerance Mechanisms and Laboratory of Regional Resources Reassessment, Asian Natural Environmental Science Center, The University of Tokyo, for providing the microscope and assistance for root image analysis.

Disclosure statement

No potential conflict of interest was reported by the authors.

References

- Abràmoff, M. D., Magalhães, P. J., & Ram, S. J. (2005). Image processing with ImageJ. *Biophotonics International*, 11(7), 36–43.
- Atkinson, J. A., & Wells, D. M. (2017). An updated protocol for high throughput plant tissue sectioning. *Frontiers in Plant Science*, 8, 1721.
- Babu, R. C., Shashidhar, H. E., Lilley, J. M., Thanh, N. D., Ray, J. D., Sadasivam, S., ... Nguyen, H. T. (2001). Variation in root penetration ability, osmotic adjustment and dehydration tolerance among accessions of rice adapted to rainfed lowland and upland ecosystems. *Plant Breeding*, 120(3), 233–238.
- Burton, A. L., Williams, M., Lynch, J. P., & Brown, K. M. (2012). RootScan: Software for high-throughput analysis of root anatomical traits. *Plant and Soil*, 357(1), 189–203.
- Chopin, J., Laga, H., Huang, C. Y., Heuer, S., & Miklavcic, S. J. (2015). RootAnalyzer: A cross-section image analysis tool for automated characterization of root cells and tissues. *PLoS One*, 10(9), e0137655.
- Deshmukh, V., Kamoshita, A., Norisada, M., & Uga, Y. (2017). Near-isogenic lines of IR64 (*Oryza sativa* subsp. *indica* cv.) introgressed with *DEEPER ROOTING 1* and *STELE TRANSVERSAL AREA 1* improve rice yield formation over the background parent across three water management regimes. *Plant Production Science*, 20(3), 249–261.
- Hazman, M., & Brown, K. M. (2018). Progressive drought alters architectural and anatomical traits of rice roots. *Rice*, 11(1), 62.
- Henry, A., Cal, A. J., Batoto, T. C., Torres, R. O., & Serraj, R. (2012). Root attributes affecting water uptake of rice (*Oryza sativa*) under drought. *Journal of Experimental Botany*, 63(13), 4751–4763.
- Jeong, J. S., Kim, Y. S., Redillas, M. C., Jang, G., Jung, H., Bang, S. W., ... Kim, J. K. (2013). OsNAC5 overexpression enlarges root diameter in rice plants leading to enhanced drought tolerance and increased grain yield in the field. *Plant Biotechnology Journal*, 11(1), 101–114.
- Jongdee, B., Fukai, S., & Cooper, M. (2002). Leaf water potential and osmotic adjustment as physiological traits to improve drought tolerance in rice. *Field Crops Research*, 76(2–3), 153–163.
- Kadam, N. N., Yin, X., Bindraban, P. S., Struik, P. C., & Jagadish, K. S. V. V. (2015). Does morphological and anatomical plasticity during the vegetative stage make wheat more tolerant of water deficit stress than rice? *Plant Physiology*, 167(4), 1389–1401.

- Kato, Y., Kamoshita, A., & Yamagishi, J. (2007). Evaluating the resistance of six rice cultivars to drought: root restriction and the use of raised beds. *Plant and Soil*, 300, 149–161.
- Kondo, M., Aguilar, A., Abe, J., & Morita, S. (2000). Anatomy of nodal roots in tropical upland and lowland rice varieties. *Plant Production Science*, 3(4), 437–445.
- Mackill, D. J., & Khush, G. S. (2018). IR64: A high-quality and high-yielding mega variety. *Rice*, 11(1), 18.
- Miyamoto, N., Steudle, E., Hirasawa, T., & Lafitte, R. (2001). Hydraulic conductivity of rice roots. *Journal of Experimental Botany*, 52(362), 1835–1846.
- Morita, S., & Nemoto, K. (1995). Morphology and anatomy of rice roots with special reference to coordination in organo- and histogenesis. In F. Baluska, Ciamporová, M., Gasparíková, O., & Barlow, P. W. (Ed.), *Structure and function of roots* (pp. 75–86). Springer, Dordrecht, Netherlands.
- Nemoto, H., Suga, R., Ishihara, M., & Okutsu, Y. (1998). Deep rooted rice varieties detected through the observation of root characteristics using the trench method. *Breeding Science*, 48(3), 321–324.
- Oyanagi, A., Nakamoto, T., & Wada, M. (1993). Relationship between root growth angle of seedlings and vertical distribution of roots in the field in wheat cultivars. *Japanese Journal of Crop Science*, 62(4), 565–570.
- Ramalingam, P., Kamoshita, A., Deshmukh, V., & Uga, Y. (2017). Association between root growth angle and root length density of a near-isogenic line of IR64 rice with *DEEPER ROOTING 1* under different levels of soil compaction. *Plant Production Science*, 20(2), 162–175.
- Rebouillat, J., Dievart, A., Verdeil, J. L., Escoute, J., Giese, G., Breitler, J. C., ... Périn, C. (2009). Molecular genetics of rice root development. *Rice*, 2(1), 15–34.
- Richards, R. A., & Passioura, J. B. (1989). A breeding program to reduce the diameter of the major xylem vessel in the seminal roots of wheat and its effect on grain yield in rain-fed environments. *Australian Journal of Agricultural Research*, 40(5), 943–950.
- Rieger, M., & Litvin, P. (1999). Root system hydraulic conductivity in species with contrasting root anatomy. *Journal of Experimental Botany*, 50(331), 201–209.
- Schneider, C. A., Rasband, W. S., & Eliceiri, K. W. (2012). NIH image to ImageJ: 25 years of image analysis. *Nature Methods*, 9(7), 671–675.
- Sibounheuang, V., Basnayake, J., & Fukai, S. (2006). Genotypic consistency in the expression of leaf water potential in rice (*Oryza sativa* L.). *Field Crops Research*, 97(2–3), 142–154.
- Terashima, K., Hiraoka, H., & Nishiyama, I. (1987). Varietal difference in the root of rice plant. I. Varietal difference in the morphology of crown root. *Japanese Journal of Crop Science*, 56(4), 521–529.
- Uga, Y., Ebana, K., Abe, J., Morita, S., Okuno, K., & Yano, M. (2009). Variation in root morphology and anatomy among accessions of cultivated rice (*Oryza sativa* L.) with different genetic backgrounds. *Breeding Science*, 59(1), 87–93.
- Uga, Y., Okuno, K., & Yano, M. (2008). QTLs underlying natural variation in stele and xylem structures of rice root. *Breeding Science*, 58(1), 7–14.
- Uga, Y., Okuno, K., & Yano, M. (2010). Fine mapping of *Sta1*, a quantitative trait locus determining stele transversal area, on rice chromosome 9. *Molecular Breeding*, 26(3), 533–538.
- Uga, Y., Sugimoto, K., Ogawa, S., Rane, J., Ishitani, M., Hara, N., ... Yano, M. (2013). Control of root system architecture by *DEEPER ROOTING 1* increases rice yield under drought conditions. *Nature Genetics*, 45(9), 1097–1102.
- Voss-Fels, K. P., Snowdon, R. J., & Hickey, L. T. (2018). Designer roots for future crops. *Trends in Plant Science*, 23(11), 957–960.
- Yaginuma, S. (2017). *On-farm evaluation of near-isogenic lines of rice with different heading dates and root traits in a paddy in Arakawa Alluvial Plain* (Master thesis). The University of Tokyo, Tokyo, Japan (in Japanese).
- Yamagishi, J., Nakamoto, T., & Richner, W. (2003). Stability of spatial variability of wheat and maize biomass in a small field managed under two contrasting tillage systems over 3 years. *Field Crops Research*, 81(2–3), 95–108.
- Yambao, E. B., Ingram, K. T., & Real, J. G. (1992). Root xylem influence on the water relations and drought resistance of rice. *Journal of Experimental Botany*, 43(7), 925–932.
- Yoshida, S., & Hasegawa, S. (1982). The rice root system: Its development and function. In R. Baxter, N. Hastings, A. Law, & E. J. Glass (Eds.), *Drought resistance in crops with emphasis on rice* (Vol. 39, pp. 561–563). IRRI, Los Baños, Philippines.
- Y, P. (2019). *Eco-physiological evaluation of stele size among rice genotypes* (Master thesis). The University of Tokyo, Tokyo, Japan